

ARMY RESEARCH LABORATORY



Unsteady Flow Computations of a Finned Body in Supersonic Flight

by Jubaraj Sahu

ARL-TR-4230

August 2007

NOTICES

Disclaimers

The findings in this report are not to be construed as an official Department of the Army position unless so designated by other authorized documents.

Citation of manufacturer's or trade names does not constitute an official endorsement or approval of the use thereof.

DESTRUCTION NOTICE—Destroy this report when it is no longer needed. Do not return it to the originator.

Army Research Laboratory

Aberdeen Proving Ground, MD 21005-5066

ARL-TR-4230

August 2007

Unsteady Flow Computations of a Finned Body in Supersonic Flight

Jubaraj Sahu

Weapons and Materials Research Directorate, ARL

REPORT DOCUMENTATION PAGE			<i>Form Approved</i> <i>OMB No. 0704-0188</i>	
Public reporting burden for this collection of information is estimated to average 1 hour per response, including the time for reviewing instructions, searching existing data sources, gathering and maintaining the data needed, and completing and reviewing the collection information. Send comments regarding this burden estimate or any other aspect of this collection of information, including suggestions for reducing the burden, to Department of Defense, Washington Headquarters Services, Directorate for Information Operations and Reports (0704-0188), 1215 Jefferson Davis Highway, Suite 1204, Arlington, VA 22202-4302. Respondents should be aware that notwithstanding any other provision of law, no person shall be subject to any penalty for failing to comply with a collection of information if it does not display a currently valid OMB control number. PLEASE DO NOT RETURN YOUR FORM TO THE ABOVE ADDRESS.				
1. REPORT DATE (DD-MM-YYYY) August 2007		2. REPORT TYPE Final		3. DATES COVERED (From - To) March 2006 to June 2007
4. TITLE AND SUBTITLE Unsteady Flow Computations of a Finned Body in Supersonic Flight			5a. CONTRACT NUMBER	
			5b. GRANT NUMBER	
			5c. PROGRAM ELEMENT NUMBER	
6. AUTHOR(S) Jubaraj Sahu (ARL)			5d. PROJECT NUMBER 622618AH80	
			5e. TASK NUMBER	
			5f. WORK UNIT NUMBER	
7. PERFORMING ORGANIZATION NAME(S) AND ADDRESS(ES) U.S. Army Research Laboratory Weapons and Materials Research Directorate Aberdeen Proving Ground, MD 21005-5069			8. PERFORMING ORGANIZATION REPORT NUMBER ARL-TR-4230	
9. SPONSORING/MONITORING AGENCY NAME(S) AND ADDRESS(ES)			10. SPONSOR/MONITOR'S ACRONYM(S)	
			11. SPONSOR/MONITOR'S REPORT NUMBER(S)	
12. DISTRIBUTION/AVAILABILITY STATEMENT Approved for public release; distribution is unlimited.				
13. SUPPLEMENTARY NOTES				
14. ABSTRACT This report describes a multidisciplinary computational study undertaken to compute the flight trajectories and simultaneously predict the unsteady free flight aerodynamics of a finned projectile at supersonic speeds with the use of an advanced unstructured time-accurate Navier-Stokes computational technique. Actual flight trajectories are computed with an advanced coupled computational fluid dynamics (CFD)-rigid body dynamics (RBD) technique. In addition, our goal is to be able to extract the aerodynamic coefficients from these fully coupled time-accurate CFD-RBD computations. Computed positions and orientations of the projectile have been compared with actual data measured from free flight tests and are found to be generally in good agreement. Unsteady numerical results obtained from the coupled method and unstructured grids show the flow field, the extracted aerodynamic forces and moments, and the flight trajectories of the projectile. Aerodynamic coefficients such as the dynamic derivatives have been obtained with a separate unsteady time-accurate CFD approach and have been compared with the extracted aerodynamic coefficients from the fully coupled dynamic simulations.				
15. SUBJECT TERMS coupled CFD-RBD; flow control; pitch damping; projectile aerodynamics; time accurate				
16. SECURITY CLASSIFICATION OF:			17. LIMITATION OF ABSTRACT SAR	18. NUMBER OF PAGES 30
a. REPORT Unclassified	b. ABSTRACT Unclassified	c. THIS PAGE Unclassified		
			19b. TELEPHONE NUMBER (Include area code) 410-278-3707	

Contents

List of Figures	iv
List of Tables	iv
Acknowledgments	v
1. Introduction	1
2. Solution Technique	2
2.1 Dual Time Stepping.....	3
2.2 Grid Movement	3
2.3 Six-Degrees-of-Freedom Coupling	4
3. Results and Discussion	5
4. Summary and Conclusions	16
5. References	17
Distribution List	19

List of Figures

Figure 1. Six-DOF schematic.	4
Figure 2. Finned configuration.	6
Figure 3. Unstructured mesh near the finned body.....	6
Figure 4. Computed pressure contours.	7
Figure 5. Euler pitch angle versus x-distance.	8
Figure 6. Euler yaw angle versus x-distance.	8
Figure 7. Motion plot (a) computation, (b) flight test.....	9
Figure 8. Total aerodynamic forces (F_x , F_y , and F_z from top to bottom) versus x-distance, initial $M = 3.0$	12
Figure 9. Total aerodynamic moments (M_x , M_y , and M_z from top to bottom) versus x-distance, initial $M = 3.0$	13
Figure 10. Aerodynamic forces versus x-distance.....	14
Figure 11. Time history of the pitching moment coefficient with angle of attack in the pitch cycle, $M = 3.0$	15
Figure 12. Pitching moment coefficient versus Mach number.....	15
Figure 13. Pitch damping moment coefficient versus Mach number.....	16

List of Tables

Table 1. Comparison of extracted aerodynamic coefficients with test data.	10
--	----

Acknowledgments

This work was accomplished as part of a grand challenge project jointly sponsored by the Department of Defense High Performance Computing Modernization program and the U.S. Army Research Laboratory (ARL). The author wishes to thank Dr. Sukumar Chakravarthy of the Metacomp Technologies for his technical assistance on some of the issues for unsteady flow simulations using CFD++ code. The author also wishes to thank Mr. Wayne Hathaway of Arrow Tech Associates and Prof. Mark Costello of the Georgia Institute of Technology for their help with the fitting of the CFD-generated data and extraction of aerodynamic coefficients. The scientific visualization and the computational support of ARL's Major Shared Resource Center are greatly appreciated.

INTENTIONALLY LEFT BLANK.

1. Introduction

The prediction of aerodynamic coefficients for projectile configurations is essential in the assessment of the performance of new designs. Understanding the aerodynamics of projectiles, rockets, and missiles is critical to the design of stable configurations and contributes significantly to the overall performance of weapon systems (*1 through 3*). The prediction of aerodynamic coefficients for these weapon systems is essential in the assessment of the performance of new designs. Numerical simulations have the potential of greatly reducing design costs while providing a detailed understanding of the complex aerodynamics associated with each change. Recently, we have made progress in coupling computational fluid dynamics (CFD) and flight dynamics to perform required multidisciplinary simulations for moving body problems. This involves real-time multidisciplinary coupled CFD-rigid body dynamic (RBD) computations for the entire flight trajectory of a complex guided projectile system. This can lead to accurate determination of aerodynamics, critical to the low-cost development of new advanced guided projectiles, rockets, missiles, and smart munitions.

Improved computer technology and state-of-the-art numerical procedures now enable solutions to complex, three-dimensional (3-D) problems associated with projectile and missile aerodynamics. In particular, our recent focus has been directed at the development and application of advanced predictive capabilities to compute unsteady projectile aerodynamics, especially during and after control maneuvers. During these maneuvers (*4, 5*) very limited data are available, and there is a lack of knowledge and understanding of the detailed aerodynamics. Accurate numerical modeling of the unsteady aerodynamics has been found to be challenging and has required the use of time-accurate solutions techniques. The present work is focused on the coupling of CFD and RBD techniques for simultaneous prediction of the unsteady free-flight aerodynamics and the flight trajectory of projectiles. In addition, our goal in the future is to be able to perform time-accurate multidisciplinary coupled CFD-RBD computations for complex guided projectiles with control maneuvers using control surfaces such as fins and canards.

Multidisciplinary computations can provide detailed fluid dynamic understanding of the unsteady aerodynamic processes involving the maneuvering flight of modern guided weapon systems. The advanced CFD capability used here solves the unsteady Navier-Stokes equations (*6 through 8*), incorporates unsteady boundary conditions and a special coupling procedure. The present research allows “virtual fly-out” of projectiles on the supercomputers and allows numerical prediction of the actual flight paths of a projectile and all the associated unsteady free flight aerodynamics using coupled CFD-RBD techniques in an integrated manner. Sahu (*9*) has successfully applied such advanced coupled procedures to simultaneously determine the flight trajectory and the associated unsteady free-flight aerodynamics of a finned projectile at supersonic velocity using structured grids. This research work was further extended and applied to a spinning projectile at a subsonic

speed with and without flow control (10). The present research two purposes: to use unstructured methodology to perform similar virtual fly-outs with the use of unstructured grids, and to develop and apply methods to extract the aerodynamic coefficients, including the dynamic pitch-damping and roll-damping derivatives, and to compare the results with those obtained from the fully coupled virtual fly-outs. The following sections describe the coupled numerical procedure and the computed results obtained for the finned body at supersonic speeds.

2. Solution Technique

At the U.S. Army Research Laboratory, research efforts are continuing to perform real-time multidisciplinary coupled CFD-RBD computations for the entire flight trajectory of a complex guided projectile system. A real-time accurate approach is used in the present work; however, the computations require much greater computer resources. The real-time accurate approach requires that the six-degrees-of-freedom (6-DOF) body dynamics be computed at each repetition of a flow solver. The CFD capability used here solves the Navier-Stokes equations and incorporates advanced boundary conditions and grid motion capabilities. The complete set of 3-D time-dependent Navier-Stokes equations is solved in a time-accurate manner for simulations of actual flights. A commercially available code, CFD++ (7, 8) is used for the time-accurate unsteady CFD simulations. The basic numerical framework in the code contains unified grid, unified physics, and unified computing features. The user is referred to these references for details of the basic numerical framework.

The 3-D, time-dependent Reynolds-averaged Navier-Stokes (RANS) equations are solved with the following finite volume method:

$$\frac{\partial}{\partial t} \int_V \mathbf{W} dV + \oint [\mathbf{F} - \mathbf{G}] \cdot d\mathbf{A} = \int_V \mathbf{H} dV \quad (1)$$

in which \mathbf{W} is the vector of conservative variables, \mathbf{F} and \mathbf{G} are the inviscid and viscous flux vectors, respectively, \mathbf{H} is the vector of source terms, V is the cell volume, and A is the surface area of the cell face.

The use of an implicit scheme circumvents the stringent stability limits encountered by their explicit counterparts, and successive relaxation allows cells to be revised as information becomes available and thus aids convergence. These features of the code have been extremely useful in the present numerical simulations at supersonic speeds. Second order discretization was used for the flow variables and the turbulent viscosity equation. The turbulence closure is based on topology-parameter-free formulations. Two-equation turbulence models (11, 12) were used for the computation of turbulent flows. These models are ideally suited to unstructured bookkeeping and

massively parallel processing because of their independence from constraints related to the placement of boundaries and/or zonal interfaces.

For time-accurate simulations of virtual fly-outs that are of interest here, dual time stepping as described next was used to achieve the desired time accuracy. The grid was actually moved to take into account the spinning motion of the projectile.

2.1 Dual Time Stepping

The “dual time-stepping mode” of the code was used to perform the transient flow simulations. The term “dual time step” implies the use of two time steps. The first is an “outer” or global (and physical) time step that corresponds to the time discretization of the physical time variation term. This time step can be chosen directly by the user and is typically set to a value to represent 1/100 of the period of oscillation expected or forced in the transient flow. It is also applied to every cell and is not spatially varying.

An artificial or “inner” or “local” time variation term is added to the basic physical equations. This time step and corresponding “inner iteration” strategy is chosen to help satisfy the physical transient equations to the desired degree. If the inner iterations converge, then the outer physical transient equations (or their discretization) are satisfied exactly; otherwise, they are satisfied approximately. For the inner iterations, the time step is allowed to vary spatially. Also, relaxation with multi-grid (algebraic) acceleration is employed to reduce the residues of the physical transient equations. It is found that an order of magnitude reduction in the residues is usually sufficient to produce a good transient iteration. This may require a few internal iterations (between 3 and 10) to achieve, depending on the magnitude of the outer time step, the nature of the problem, the nature of the boundary conditions, and the consistency of the mesh with respect to the physics at hand.

2.2 Grid Movement

Grid velocity is assigned to each mesh point. This general capability can be tailored for many specific situations. For example, the grid point velocities can be specified to correspond to a spinning projectile. In this case, the grid speeds are assigned as if the grid were attached to the projectile and spinning with it. Similarly, to account for RBD, the grid point velocities can be set as if the grid were attached to the rigid body with 6 DOF. As shown in figure 1, the 6 DOF includes the inertial position components of the projectile mass center (x, y, z) and the three standard Euler angles (ϕ, θ, ψ): roll angle, pitch angle, and yaw angle, respectively. For RBD, the coupling refers to the interaction between the aerodynamic forces and moments and the dynamic response of the projectile and body to these forces and moments. The forces and moments are computed every CFD time step and transferred to a 6-DOF module that computes the body’s response to the forces and moments. The response is converted into translational and rotational accelerations that are integrated to obtain translational and rotational velocities and integrated once more to obtain linear position and angular orientation. The 6-DOF RBD module uses quaternions to define the angular

orientations. However, these are easily translated into Euler angles. From the dynamic response, the grid point locations and grid point velocities are set.

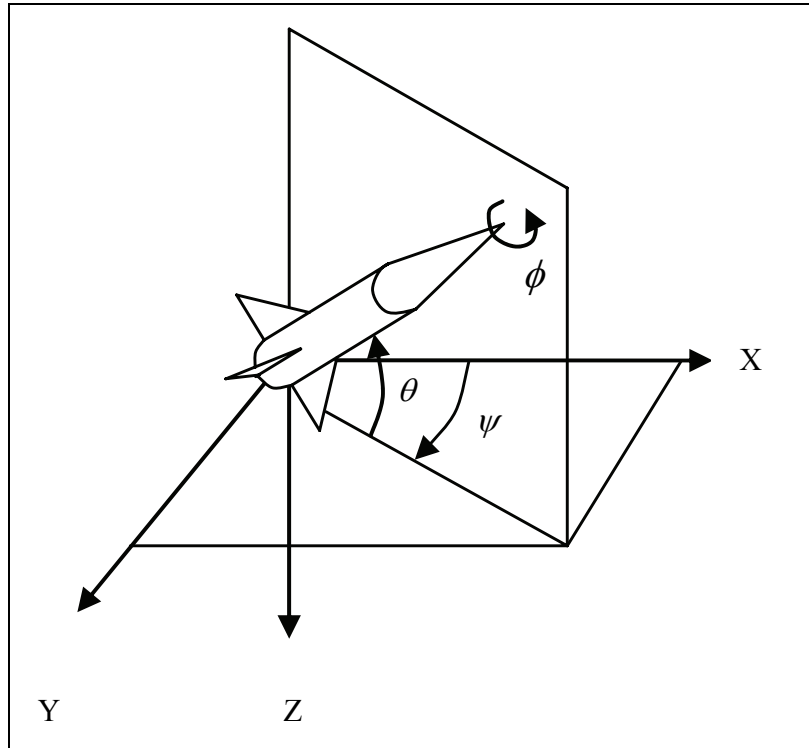


Figure 1. Six-DOF schematic.

2.3 Six-Degrees-of-Freedom Coupling

In CFD++, two modes are available to help simulate RBD: an uncoupled mode and a coupled mode. The coupling refers to the interaction between the aerodynamic forces and moments and the dynamic response of the projectile or body to these forces and moments. In both modes, the forces and moments are computed every time step and reported to the user. In the coupled mode, the forces and moments are passed to a 6-DOF module which computes the body's response to the forces and moments. The response is converted into translational and rotational accelerations which are integrated to result in translational and rotational velocities and integrated once more to result in linear position and angular orientation. The 6-DOF RBD module uses quaternions to define the angular orientations. However, these are easily translated into Euler angles. From the dynamic response, the grid point locations and grid point velocities are set. In the uncoupled mode, the forces and moments are not coupled with the RBD module. The motion of the projectile is kinematics only and depends on the initial linear and angular velocities prescribed.

The projectile state vector consists of the inertial position components of the projectile mass center (x,y,z) , the standard Euler angles (ϕ, θ, ψ) , the body frame components of the projectile mass center velocity (u,v,w) , and the body frame components of the projectile angular velocity vector (p,q,r) .

The entire state vector consisting of these 12 variables is required in the initial conditions before a virtual fly-out can be performed and a coupled dynamic solution can be obtained. Typically, we begin with a computation performed in “steady state mode” with the grid velocities prescribed to account only for the translational motion component of the complete set of initial conditions to be prescribed. At this stage, we also impose the angular orientations from the initial conditions. The complete set of initial conditions includes translational and rotational velocity components along with initial position and angular orientation. With a fixed translational velocity, we obtain the steady state solution. This becomes the initial condition for the next step which involves adding just the spin component of the projectile. With the addition of spin, time-accurate calculations are performed for a few cycles of spin until converged periodic forces and moments are obtained. A sufficient number of time steps are performed so that the angular orientation for the spin axis corresponds to the prescribed initial conditions. All this is performed in an uncoupled mode. The angular velocity initial conditions associated with the non-spin rotational modes are then added. The mesh is translated back to the desired initial position, the non-spin rotational velocity initial conditions are turned on, and computations are performed in the coupled mode.

As a special case, this procedure can also be run very easily in an uncoupled mode to model motions such as the pitching and rolling of a projectile. Such a time-accurate CFD procedure allows one to compute the dynamic derivatives of projectiles from the unsteady simulations. For determination of dynamic derivatives, all calculations are done only in the uncoupled mode. In addition, the translational velocity is fixed to zero. The spin component of the projectile or the angular velocity of the projectile is added to compute the rolling motion of the projectile. With the addition of spin, time-accurate calculations are performed for a few cycles of spin until converged periodic forces and moments are obtained. A sufficient number of time steps are similarly performed for the angular pitching motion case where the pitching motion (sinusoidal, for example) is imposed.

3. Results and Discussion

Time-accurate unsteady numerical computations were performed with Navier-Stokes and coupled 6-DOF methods to predict the flow field and aerodynamic coefficients and the flight paths of a fin-stabilized projectile at supersonic speed, $M = 3$. In all cases, full 3-D computations were performed, but no symmetry was used.

The supersonic projectile modeled in this study is an ogive-cylinder-finned configuration (see figure 2). The length of the projectile is 121 mm and the diameter is 13 mm. The ogive nose is 98.6 mm long and the afterbody has a 22.3-mm, 2.5-degree boattail. Four fins are situated on the back end of the projectile. Each fin is 22.3 mm long and 10.16 mm thick.

An unstructured computational mesh was generated for this projectile (see figure 3). In general, most of the grid points are clustered in the boundary layer as well as near the afterbody fin and the wake regions. The total number of grid points is about 6.5 million for the full grid. The first spacing away from the wall was selected to yield a y^+ value of 1.0. The projectile configuration has a base cavity and was included in the mesh generation process. The unstructured mesh also included the base cavity region and was generated with the use of the Multipurpose Intelligent Meshing Environment (MIME) grid-generation software recently developed by Metacomp Technologies.

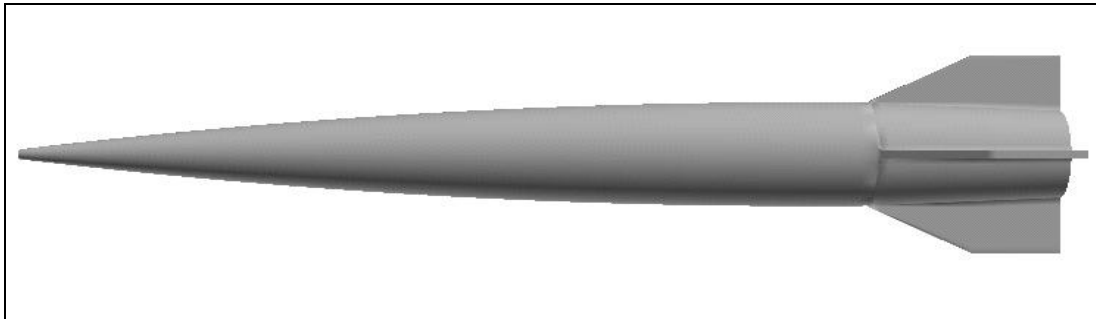


Figure 2. Finned configuration.

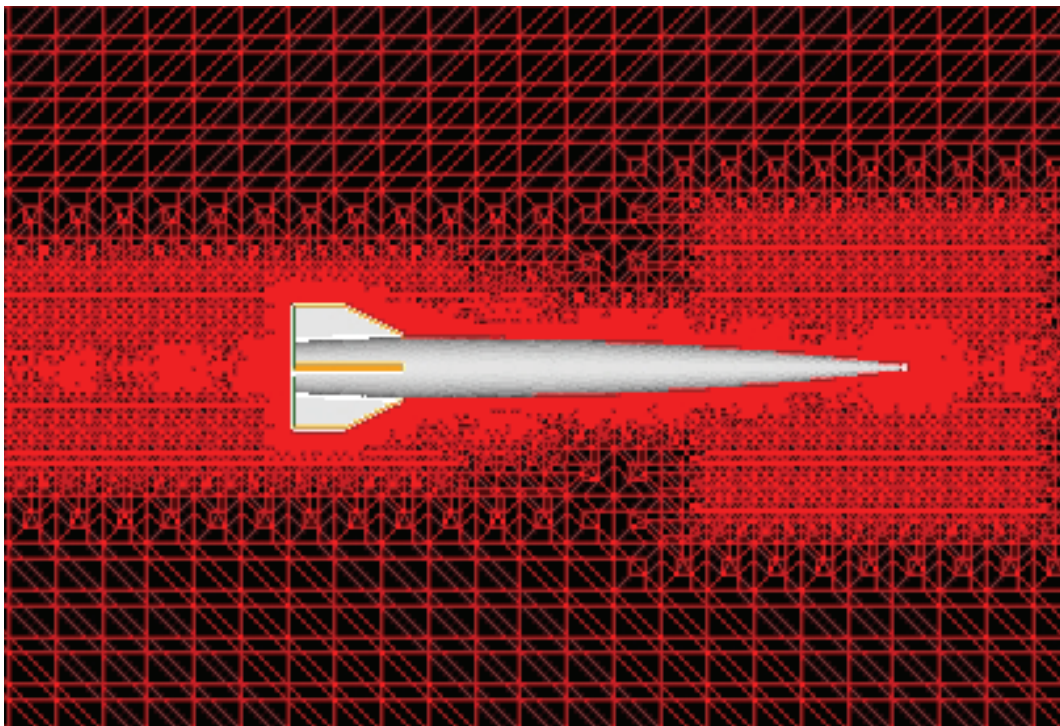


Figure 3. Unstructured mesh near the finned body.

Here, our primary interest is in the development and application of coupled CFD and RBD techniques for accurate simulation of the free flight aerodynamics and flight dynamics of the projectile in supersonic flight. The total aerodynamic forces and moments are used for the virtual

fly-outs of the projectiles. The first step was to obtain the steady state results for this projectile at a given initial supersonic velocity. Also imposed were the angular orientations at this stage. Corresponding converged steady state solution was then used as the starting condition along with the other initial conditions for the computation of coupled CFD-RBD runs. Numerical computations have been made for these cases at an initial velocity of 1034 m/s. The simulations were started a small distance away from the muzzle. The corresponding initial angle of attack was $\alpha = 4.9$ degrees and initial spin rate was 2500 rad/s. Figure 4 shows the computed pressure contours at a given time or at a given location in the trajectory. It clearly shows the orientation of the body at that instant in time and the resulting asymmetric flow field attributable to the body at angle of attack. The orientation of the projectile of course changes from one instant in time to another as the projectile flies down range. Figure 5 shows the variation of the Euler pitch angle with distance traveled. As seen in this figure, both the amplitude and frequency in the Euler angle variation are predicted very well by the computed results and match extremely well with the data from the flight tests. One can also clearly see that the amplitude damps as the projectile flies down range, i.e., with the increasing x-distance. As shown in figure 6, similar behavior is observed with the Euler yaw angle, and it damps with the increasing x-distance. Computed results again compare very well with the measured data from the flight tests.

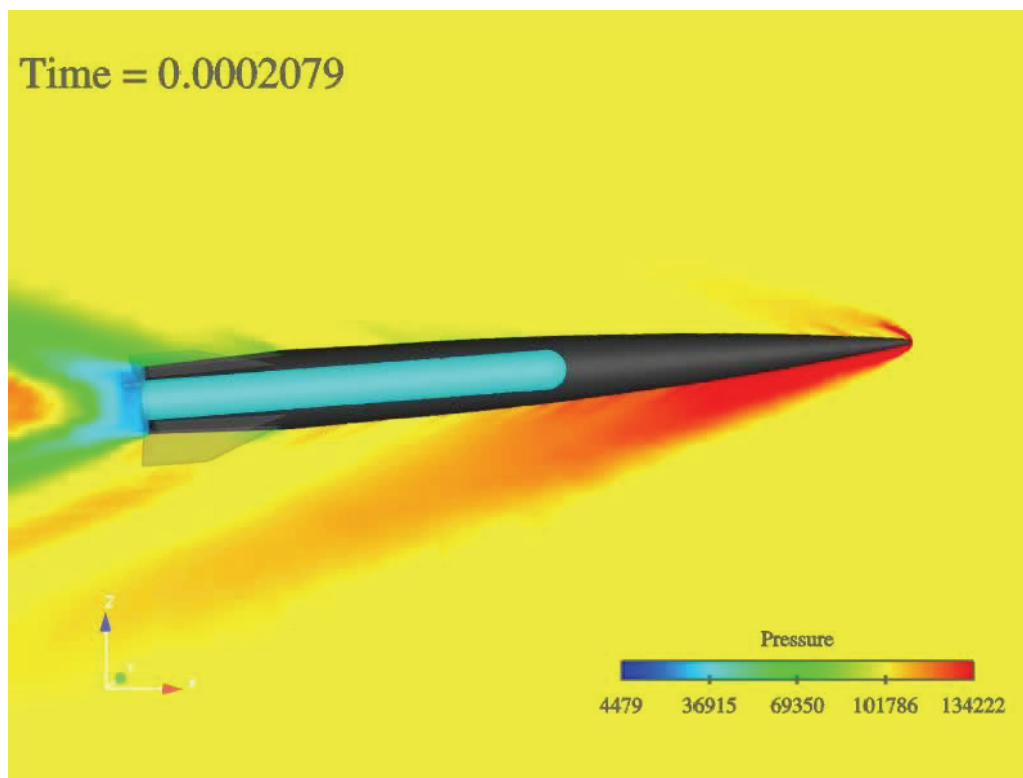


Figure 4. Computed pressure contours.

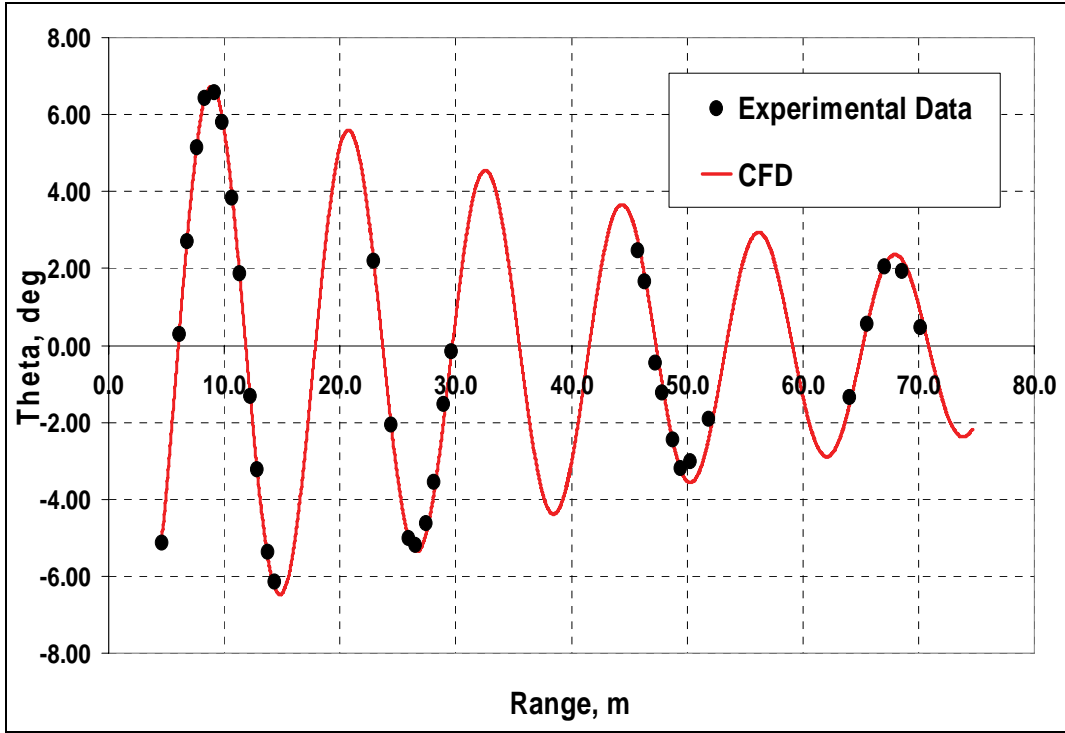


Figure 5. Euler pitch angle versus x-distance.

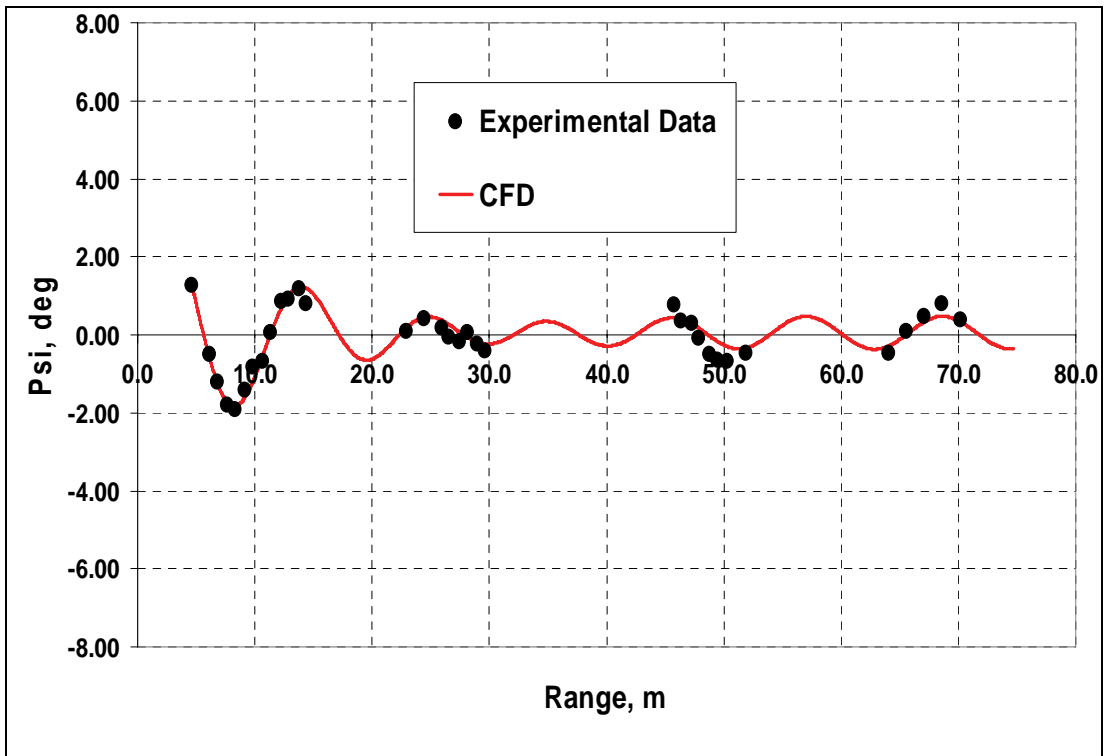


Figure 6. Euler yaw angle versus x-distance.

The time histories of the pitch and yaw angles are often customarily presented as a motion plot where the pitch angle is plotted versus the yaw angle during the flight of the projectile. It represents the path traversed by the nose of the projectile during the flight trajectory (looking forward from the back of the projectile). Such motion plots are shown in figure 7. This figure shows the comparison of the motion plots obtained from the numerical simulations and the 6-DOF analysis of the flight results from ARFDAS (Aeroballistics Research Facility Data Analysis System) (13) software commonly used for this purpose. Computed results match very well with the experimental flight test results. The unsteady simulations took thousands of hours of central processing unit time on a Xeon PC cluster system running with 32 to 64 processors.

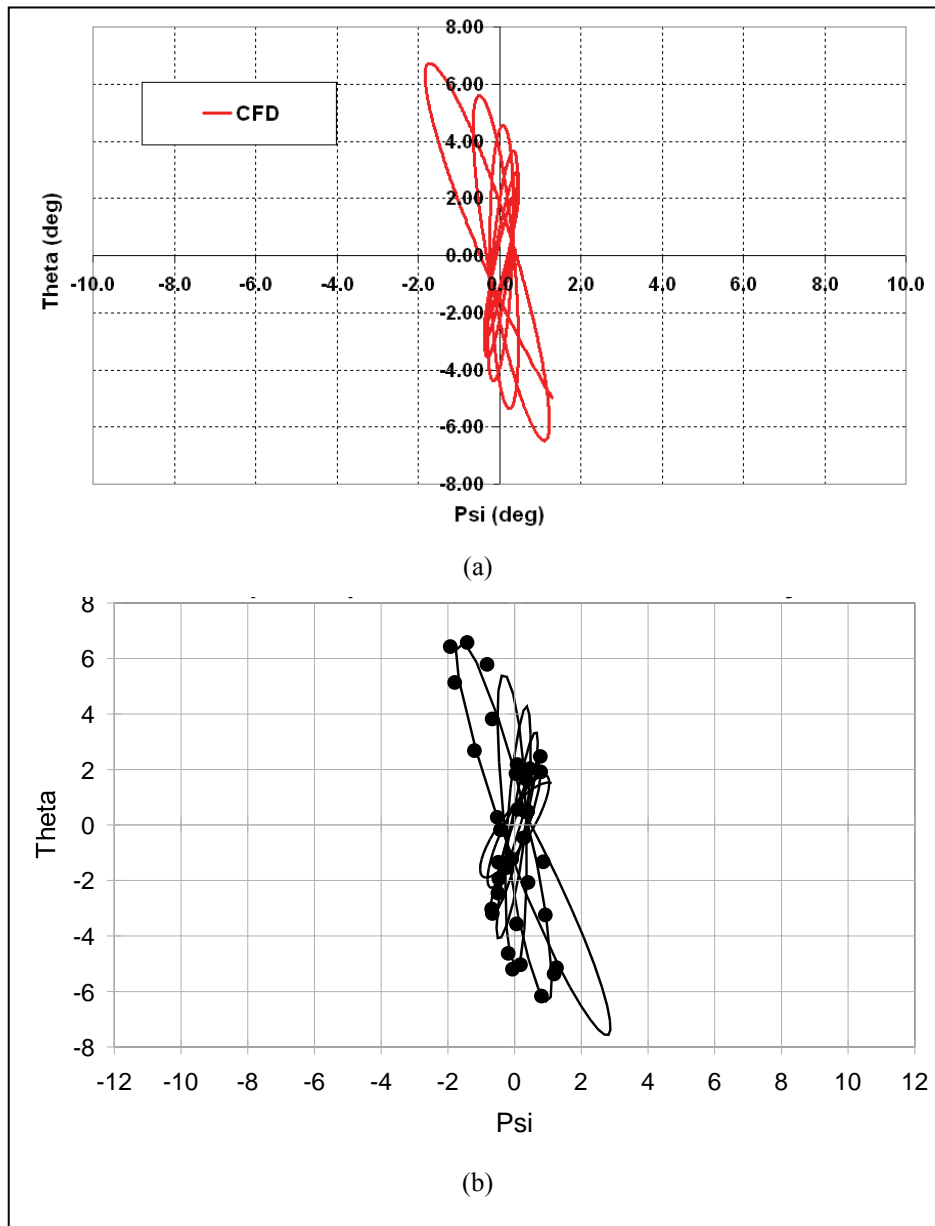


Figure 7. Motion plot (a) computation, (b) flight test.

The results produced by the virtual fly-out simulations provide the total aerodynamic forces and moments at every time step as the projectile flies down range. For a variety of reasons, one may want to extract the traditional aerodynamic force and moment coefficients from these coupled CFD-RBD simulations. For example, the aerodynamic coefficients are in many cases available from experiments and other databases and can be used for further verification and validation of the computed results obtained from the virtual fly-out simulations. Currently, work is in progress to look at a number of ways to achieve it. One way is to feed the CFD-RBD-generated data back into software such as ARFDAS and extract the aerodynamic coefficients with the same procedure used on the actual test data (14). Another approach is to perform a set of short time histories or virtual fly-outs at different Mach numbers and use a simple fitting procedure to estimate all aerodynamic force and moment coefficients (15).

Both approaches were used in this study to extract the aerodynamic force and moment coefficients for the finned projectile. In the first approach, the position (x,y,z) and the orientation (three Euler angles) of the projectile, obtained from the virtual fly-out simulations, were provided as input to ARFDAS. These are the six quantities that are actually measured in the free flight tests, a reduction procedure is performed, and the aerodynamics that best fit the data are obtained. The CFD-generated data were cast to resemble spark range data, and the same fitting procedure was applied. The aerodynamics that matched the CFD-supplied data were obtained and the aerodynamic coefficients were extracted (14). The second approach is currently being developed and the results, although somewhat preliminary, are included for comparison. The extracted aerodynamic coefficients are shown in table 1 and are compared with the same coefficients obtained with the actual test data. As shown in table 1, computed aerodynamic coefficients are generally in very good agreement with the data for the static aerodynamic coefficients such as the drag, normal force, and pitching moment coefficients. The table also includes a comparison of the dynamic derivatives such as the pitch-damping moment and the roll-damping derivatives. Dynamic derivatives extracted by the first approach seem to be in slightly better agreement with the data than those extracted by the second approach. As stated earlier, the second approach is still undergoing development, and its accuracy is expected to improve in the near future.

Table 1. Comparison of extracted aerodynamic coefficients with test data.

Data Source	Mach No.	Zero Yaw Axial Force Coeff, C_{X_0}	Normal Force Coeff Deriv., $C_{N\alpha}$	Pitching Moment Coeff Deriv, $C_{m\alpha}$	Pitch Damping Moment Coeff, C_{mq}	Roll Damping Moment Coeff, C_{lp}
Spark Range	3.0	0.22	5.83	-12.60	-196	-2.71
CFD (1)	3.0	0.24	5.88	-12.46	-172	-3.24
CFD (2)	3.0	0.24	5.83	-12.36	-150	-3.40

Some of the results obtained from the fitting procedure with the first approach are shown figures 8 and 9. Figure 8 shows the total aerodynamic forces in all three coordinate directions as a function of the x-distance or the range. As shown in this figure, the ARFDAS fitting procedure produces aerodynamic forces that match well with the computed results from the virtual fly-out of the projectile. As seen here, the total axial force decreases with increasing range as the total angle

of attack decreases. Initially, the angle of attack is larger and it becomes smaller and smaller, i.e., the amplitude of oscillations becomes smaller with increasing x-distance. The total force in the y-direction, F_y , is initially larger and damps some until an x-distance of about 25 m. With increasing x-distance beyond 25 m, the amplitude of oscillation stays more or less the same. As expected, the force in the z-direction, F_z , follows a trend similar to that presented earlier with the Euler pitch angle (figure 5). As the pitch angle damps with increasing x-distance, so does the amplitude of oscillation in F_z . It decreases with the increase in the range. Figure 9 shows the variation of total aerodynamic moments with the distance downrange. All the moments are taken with respect to the center of gravity of the projectile. Again, the total aerodynamic moments (M_x , M_y , and M_z) produced by the ARFDAS fitting procedure match fairly well the computed results.

The actual flight model included a base cavity which is known to have an effect on the aerodynamic axial force. In the present computations with the unstructured grid, the base cavity was modeled and the flow field inside the base cavity was computed. Figure 10 shows the total aerodynamic forces in the three coordinate directions. This figure shows the comparison of these forces with and without the base cavity with the forces obtained from ARFDAS. As expected, the force in x-direction (F_x) is affected by the cavity. The predicted F_x obtained with the base cavity matches with the ARFDAS result better than the F_x predicted without it. The extracted zero yaw axial force coefficient for the projectile without the base cavity was found to be approximately 0.28 with both aerodynamic coefficient extraction approaches. As shown in table 1, it drops to 0.24 with the base cavity. The base cavity appears to have a negligible effect on the other aerodynamic forces.

Although the fitting technique in the first approach to extract the aerodynamic force and moment coefficients has been used over the years with the flight data, further validation of the force and moment coefficients derived from the virtual fly-out CFD data is required. Traditional steady and unsteady CFD procedures can be employed to compute the aerodynamic force and moment coefficients to determine the accuracy of the extraction methods. The predicted static aerodynamic coefficients such as the axial force, normal force, and the pitching moment coefficients compare very well with those extracted from the full dynamic coupled calculation. The accuracy of the extracted dynamic derivatives must be determined. The numerical framework described in section 2 can be easily modified to not allow translational motion. This separate unsteady CFD procedure can then be used to calculate the pitch-damping moment and the roll-damping dynamic derivatives for projectiles with sinusoidal pitching motion and spin, respectively.

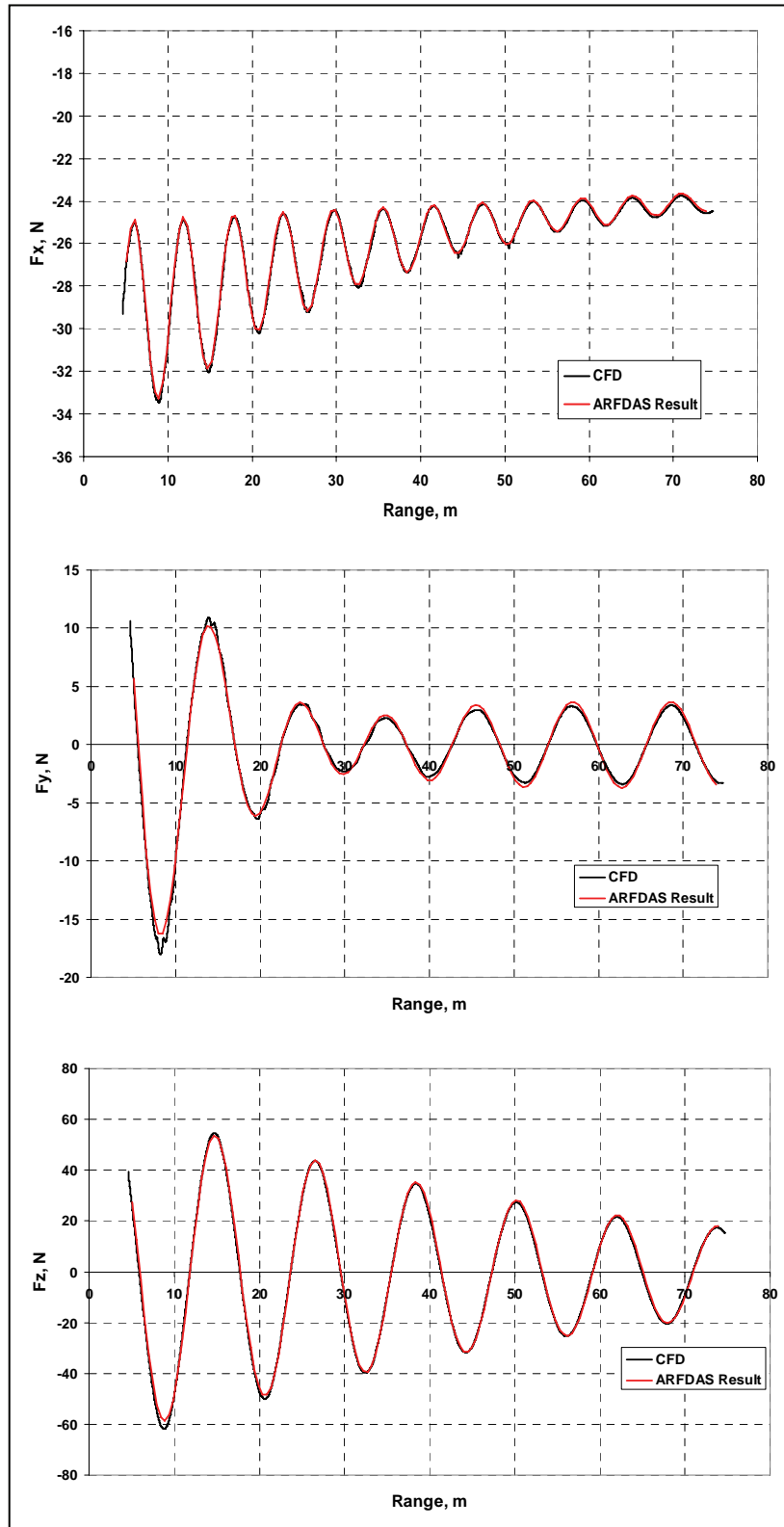


Figure 8. Total aerodynamic forces (F_x , F_y , and F_z from top to bottom) versus x-distance, initial $M = 3.0$.

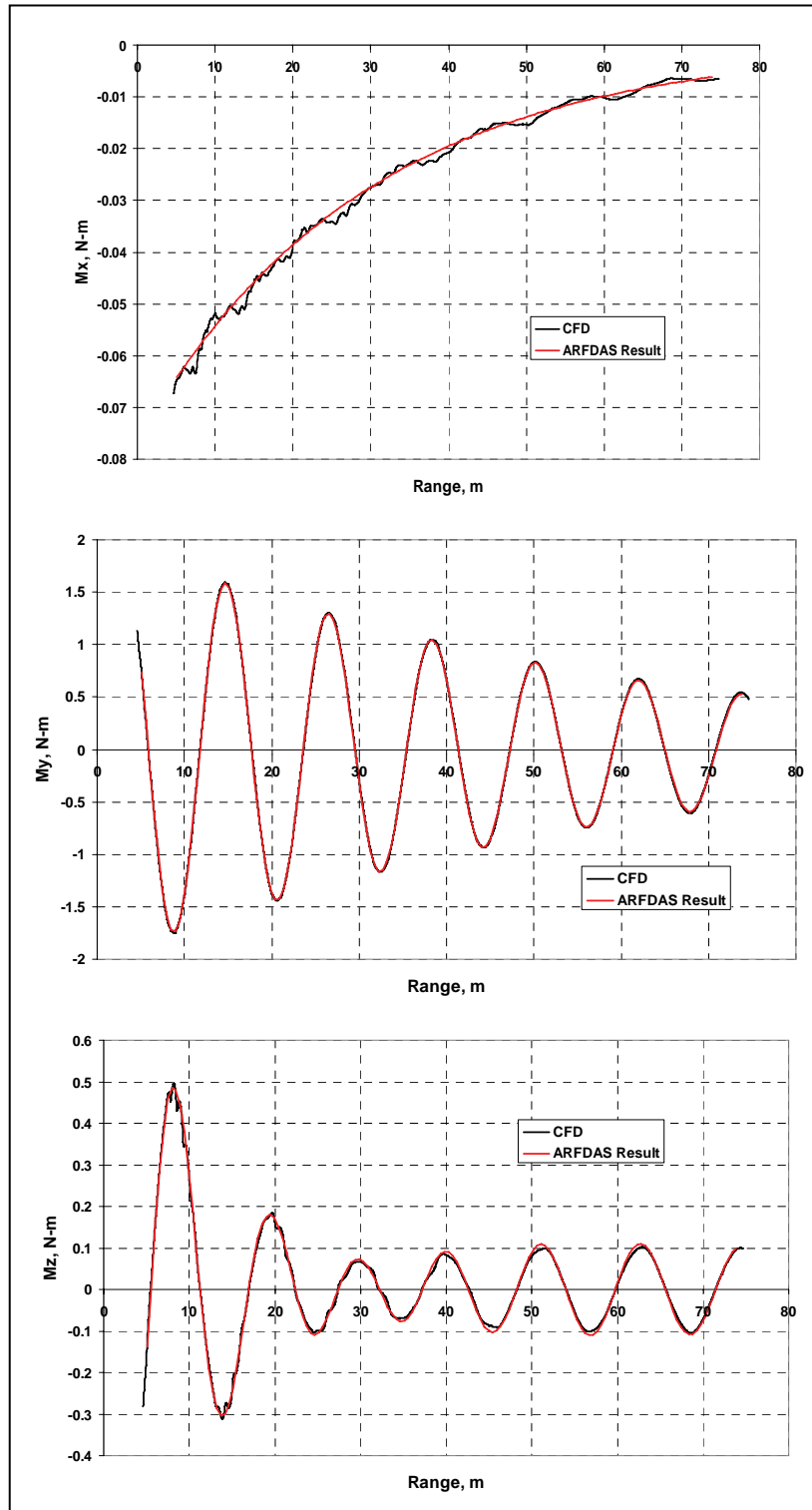


Figure 9. Total aerodynamic moments (M_x , M_y , and M_z from top to bottom) versus x-distance, initial $M = 3.0$.

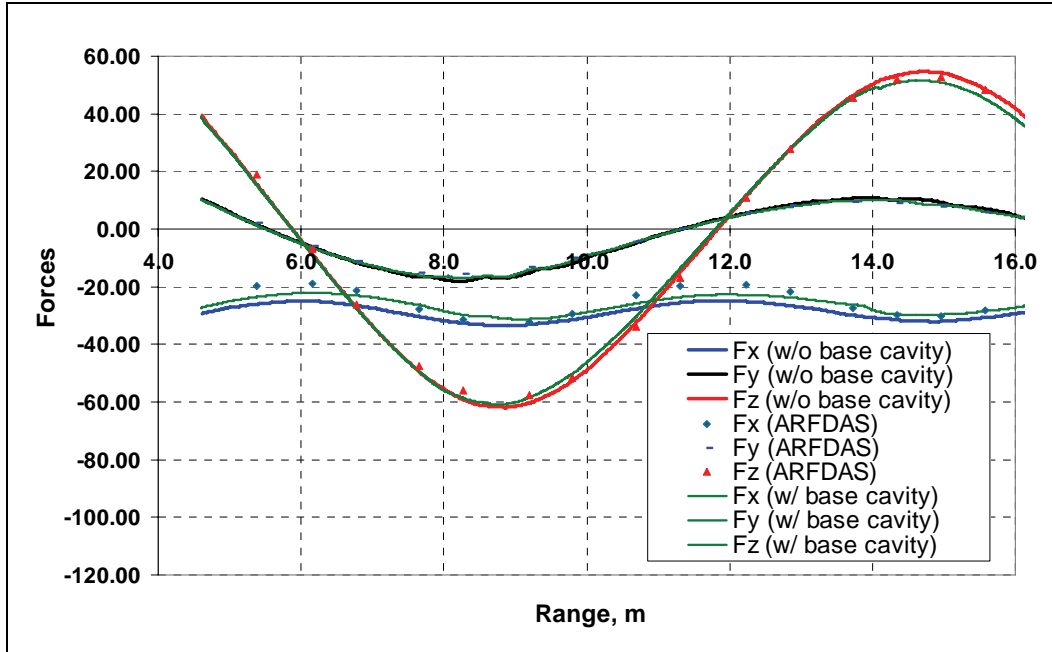


Figure 10. Aerodynamic forces versus x-distance.

In the present work, emphasis is put on the numerical computation of the pitch-damping moment coefficient and its comparison with that extracted from the virtual fly-out simulations. Sinusoidal pitching motion is imposed and time-accurate CFD computations have been performed at various supersonic velocities. Figure 11 shows the time history of the pitching moment coefficient as a function of angle of attack at $M = 3$. Computed results shown here correspond to one full cycle of imposed pitching motion and include the pitch-up and pitch-down cycles. Also shown in this figure are the computed pitching moment coefficients for the first two complete pitch cycles. Other than the initial start-up differences, the computed results converge quite rapidly at this velocity. Results obtained for the third cycle (not shown here) were virtually identical to those of the second cycle. The static pitching moment coefficient can be easily obtained from this plot if we connect a line between the two end points in the C_m curve corresponding to angles of attack of $+1$ and -1 degree and passing through the origin. The pitch-damping moment coefficient is related to the difference in the values of the pitching moment coefficients at 0 -degree angle of attack in this case between the up and down portions of the imposed pitching motion.

Computed static pitching moment coefficients as well as computed dynamic pitch-damping moment coefficients were obtained from a series of time-accurate calculations at different supersonic velocities from $M = 1.6$ to $M = 3.4$ and are shown in figures 12 and 13, respectively. These computed results are compared with the data derived from free flight tests for the same projectile configuration with single and multiple fits. Figure 12 shows the variation of the computed pitching moment coefficient with Mach number. As shown in this figure, the static pitching moment coefficient increases with Mach number from $M = 1.6$ to $M = 3.4$ and the computed results match very well with the test results. Figure 13 shows the variation of the dynamic pitch-damping moment coeffi-

cient with Mach number. Again, computed pitch-damping moment coefficients have been compared to those obtained from the flight tests for the same configuration and the same supersonic velocities. The computed results are generally in good agreement with the data and they are within the accuracy of the experimental test results. As shown in figure 13, the pitch-damping moment coefficient predicted by the separate unsteady CFD procedure at $M = 3$ is -172.5 , which is almost identical to that extracted by the first approach (see table 1) from the virtual fly-out CFD results. This result indicates that virtual fly-outs could be used to obtain the pitch-damping moment as accurately as the traditional unsteady CFD technique. Further work is needed and is currently in progress to determine the accuracy of the roll-damping coefficients and in looking at other techniques for extraction of the aerodynamic force and moment coefficients.

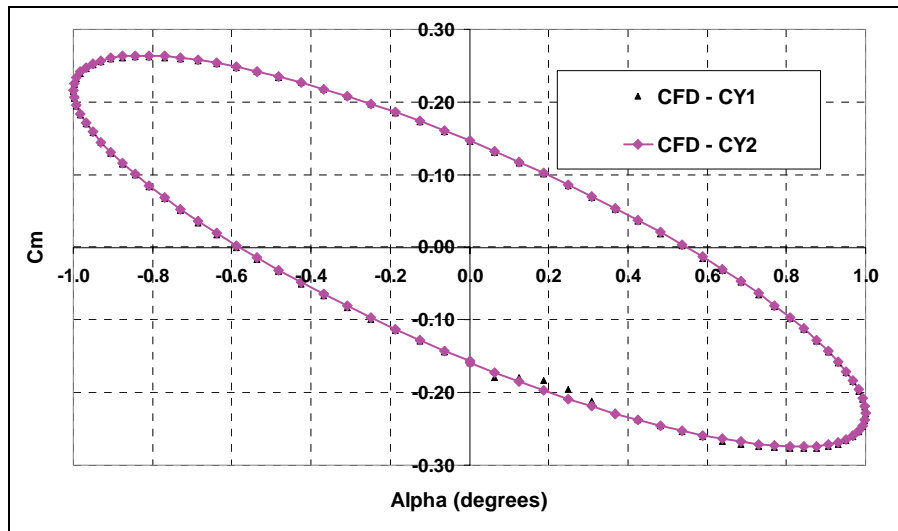


Figure 11. Time history of the pitching moment coefficient with angle of attack in the pitch cycle, $M = 3.0$.

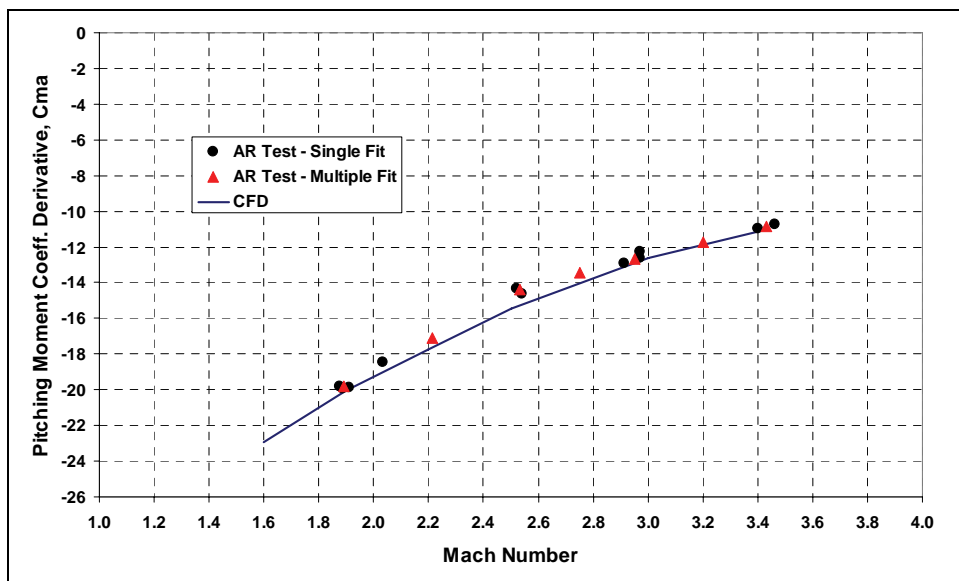


Figure 12. Pitching moment coefficient versus Mach number.

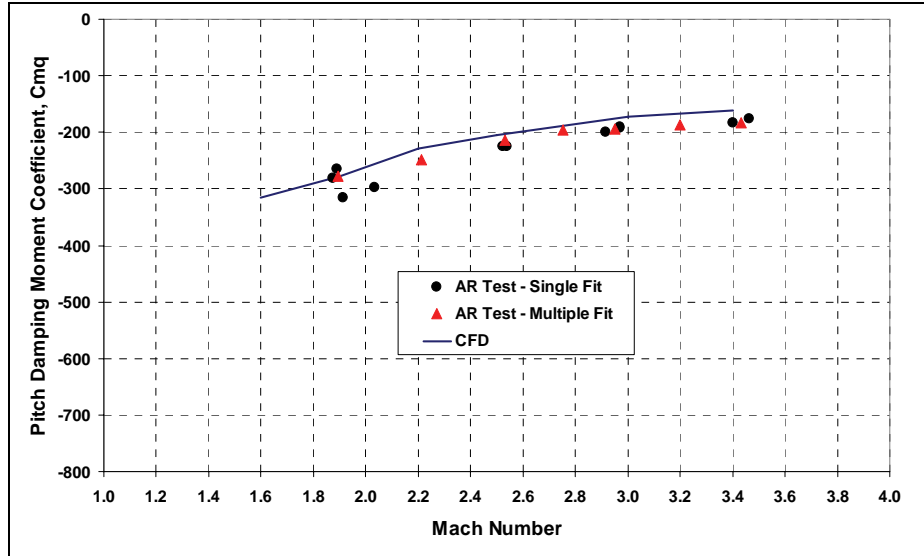


Figure 13. Pitch damping moment coefficient versus Mach number.

4. Summary and Conclusions

This report describes a coupled CFD-RBD computational study undertaken to simultaneously determine the flight trajectory and the associated unsteady free-flight aerodynamics of a finned projectile with an unstructured grid. A 3-D unsteady unstructured Navier-Stokes solver is employed to compute the time-accurate flow fields for the finned projectile at supersonic velocities. Computed results have been obtained for the virtual fly-out case an initial supersonic speed, $M = 3$ with time-accurate Navier-Stokes computational technique. Computed positions and orientations of the projectile have been compared with actual data measured from free flight tests and are found to be in good agreement. Aerodynamic force and moment coefficients have been extracted from the fully coupled CFD-RBD numerical solutions. Unsteady time-accurate CFD methods have been used separately to compute the dynamic pitch-damping moment derivatives and have been compared with those obtained from the fully coupled approach. Computed static pitching moment coefficients and dynamic pitch-damping moment derivatives have been obtained at various supersonic velocities between $M = 1.6$ and 3.4 and are found to compare well with the data obtained from free flight tests. Computed CFD results at $M = 3$ show that the pitch-damping moment derivative obtained from the virtual fly-out technique matches extremely well with that predicted by traditional unsteady CFD technique.

This work demonstrates a coupled method to accurately predict the time-accurate unsteady aerodynamics of a finned projectile at supersonic speed and provides for a new way to obtain the aerodynamic coefficients including the dynamic pitch-damping and roll-damping derivatives. The present CFD-RBD simulations clearly show the capability of the coupled approach and form the basis for future multidisciplinary, time-dependent computations of advanced maneuvering munitions.

5. References

1. Sahu, J.; Heavey, K. R.; Ferry, E. N. Computational Fluid Dynamics for Multiple Projectile Configurations. *Proceedings of the 3rd Overset Composite Grid and Solution Technology Symposium*, Los Alamos, NM, October 1996.
2. Sahu, J.; Heavey, K. R.; Nietubicz, C. J. Time-Dependent Navier-Stokes Computations for Submunitions in Relative Motion. *Sixth International Symposium on Computational Fluid Dynamics*, Lake Tahoe, NV, September 1995.
3. Meakin, R. L. *Computations of the Unsteady Flow About a Generic Wing/Pylon/Finned-Store Configuration*; AIAA 92-4568-CP; August 1992.
4. Sahu, J. *Unsteady Numerical Simulations of Subsonic Flow over a Projectile with Jet Interaction*; AIAA Paper 2003-1352; Reno, NV, 6-9 January 2003.
5. Sahu, J. *Unsteady CFD Modeling of Aerodynamic Flow Control over a Spinning Body with Synthetic Jet*; AIAA Paper 2004-0747; Reno, NV, 5-8 January 2004.
6. Pulliam, T. H.; Steger, J. L. On Implicit Finite-Difference Simulations of Three-Dimensional Flow. *AIAA Journal* **February 1982**, 18 (2), pp. 159–167.
7. Peroomian, O.; Chakravarthy, S.; Goldberg, U. A ‘Grid-Transparent’ Methodology for CFD; AIAA Paper 97-07245; 1997.
8. Peroomian, O.; Chakravarthy, S.; Palaniswamy, S.; Goldberg, U. *Convergence Acceleration for Unified-Grid Formulation Using Preconditioned Implicit Relaxation*; AIAA Paper 98-0116; 1998.
9. Sahu, J. *Time-Accurate Numerical Prediction of Free Flight Aerodynamics of a Finned Projectile*; ARL-TR-3603; U.S. Army Research Laboratory: Aberdeen Proving Ground, MD, September 2005.
10. Sahu, J. *Time-Accurate Computations of Free-Flight Aerodynamics of a Spinning Projectile With and Without Flow Control*; ARL-TR-3919; U.S. Army Research Laboratory: Aberdeen Proving Ground, MD, September 2006.
11. Goldberg, U. C.; Peroomian, O.; Chakravarthy, S. A Wall-Distance-Free K-E Model With Enhanced Near-Wall Treatment. *ASME Journal of Fluids Engineering* **1998**, 120, 457-462.
12. Batten, P.; Goldberg, U.; Chakravarthy, S. *Sub-grid Turbulence Modeling for Unsteady Flow with Acoustic Resonance*; AIAA Paper 00-0473; 38th AIAA Aerospace Sciences Meeting, Reno, NV, January 2000.

13. Arrow Tech Associates. ARFDAS Technical Manual. South Burlington, VT, 2001.
14. Wayne H. *Private communications*; Arrow Tech Associates, South Burlington, VT, June 2007.
15. Kokes, J.; Costello, M.; Sahu, J. *Generating an Aerodynamic Model for Projectile Flight Simulation Using Unsteady Time Accurate Computational Fluid Dynamic Results*; ARL-CR-577; U.S. Army Research Laboratory: Aberdeen Proving Ground, MD, September 2006.

NO. OF
COPIES ORGANIZATION

1 DEFENSE TECHNICAL
(PDF INFORMATION CTR
ONLY) DTIC OCA
8725 JOHN J KINGMAN RD
STE 0944
FORT BELVOIR VA 22060-6218

1 US ARMY RSRCH DEV & ENGRG CMD
SYSTEMS OF SYSTEMS
INTEGRATION
AMSRD SS T
6000 6TH ST STE 100
FORT BELVOIR VA 22060-5608

1 DIRECTOR
US ARMY RESEARCH LAB
IMNE ALC IMS
2800 POWDER MILL RD
ADELPHI MD 20783-1197

1 DIRECTOR
US ARMY RESEARCH LAB
AMSRD ARL CI OK TL
2800 POWDER MILL RD
ADELPHI MD 20783-1197

2 DIRECTOR
US ARMY RESEARCH LAB
AMSRD ARL CI OK T
2800 POWDER MILL RD
ADELPHI MD 20783-1197

1 AEROPREDICTION INC
F MOORE
9449 GROVER DRIVE, STE 201
KING GEORGE VA 22485

1 UNIV OF TEXAS AT ARLINGTON
MECH & AEROSPACE ENGINEERING DEPT
ATTN J C DUTTON
BOX 19018
500 W FIRST ST
ARLINGTON TX 76019-0018

2 ATK TACTICAL SYSTEMS DIV
ALLEGANY BALLISTICS LAB
ATTN D J LEWIS J S OWENS
210 STATE ROUTE 956
ROCKET CENTER WV 26726

1 ATK ADVANCED WEAPONS DIV
ATTN R H DOHRN
MN06-1000
4600 NATHAN LANE N
PLYMOUTH MN 55442

NO. OF
COPIES ORGANIZATION

1 ATK ORDNANCE SYS
ATTN B BECKER
MN07 MW44
4700 NATHAN LANE N
PLYMOUTH MN 55442

1 SCIENCE APPLICATIONS INTL CORP
ATTN J NORTHRUP
8500 NORMANDE LAKE BLVD
SUITE 1610
BLOOMINGTON MN 55437

3 GOODRICH ACTUATION SYSTEMS
ATTN T KELLY P FRANZ
J CHRISTIANA
100 PANTON ROAD
VERGENNES VT 05491

2 ARROW TECH ASSOC
ATTN W HATHAWAY J WHYTE
1233 SHELBURNE RD STE D8
SOUTH BURLINGTON VT 05403

1 KLINE ENGINEERING CO INC
ATTN R W KLINE
27 FREDON GREENDEL RD
NEWTON NJ 07860-5213

1 GEORGIA INST TECH
DEPT AEROSPACE ENGR
ATTN M COSTELLO
270 FERST STREET
ATLANTA GA 30332

1 AIR FORCE RSRCH LAB
AFRL/MNAV
ATTN G ABATE
101 W EGLIN BLVD STE 333
EGLIN AFB FL 32542-6810

1 US ARMY RDECOM ARDEC
ATTN AMSRD AAR AEM A G MALEJKO
BLDG 95
PICATINNY ARSENAL NJ 07806-5000

2 US ARMY ARDEC
ATTN AMSRD AAR AEP E D CARLUCCI
ATTN AMSRD AAR AEP E I MEHMEDAGIC
BLDG 94
PICATINNY ARSENAL NJ 07806-5000

1 US ARMY TACOM ARDEC
ATTN AMSRD AAR AEP E C KESSLER
BLDG 3022
PICATINNY ARSENAL NJ 07806-5000

NO. OF
COPIES ORGANIZATION

1 APM SMALL & MED CALIBER AMMO
OPM MAS
ATTN SFAE AMO MAS SMC
R KOWALSKI
BLDG 354
PICATINNY ARSENAL NJ 07806-5000

3 US ARMY AMRDEC
ATTN AMSAM RD SS AT L AUMAN
R W KRETZSHMAR
E VAUGHN
REDSTONE ARSENAL AL 35898-5000

ABERDEEN PROVING GROUND

1 DIRECTOR
US ARMY RSCH LABORATORY
ATTN AMSRD ARL CI OK (TECH LIB)
BLDG 4600

18 DIR USARL
AMSRD WM
J SMITH
AMSRD WM B
M ZOLTOSKI
AMSRD WM BA
D LYON
AMSRD WM BC
P PLOSTINS
I CELMINS
M CHEN
J DESPIRITO
B GUIDOS
K HEAVEY
J SAHU
S SILTON
P WEINACHT
F FRESCONI
M BUNDY
G COOPER
B HOWELL
AMSRD WM BD
B FORCH
AMSRD WM BF
J NEWILL
S WILKERSON
H EDGE

FOREIGN ADDRESSES

- 1 DSTL BEDFORD
T BIRCH
BLDG 115 RM 125
BEDFORD TECHNOLOGY PARK
BEDFORD
MK44 2FQ
UK

- 2 DEFENCE RESEARCH AND
DEVELOPMENT CANADA
VALCARTIER
F LESAGE
E FOURNIER
2459 PIE-XI BLVD NORTH
VAL BELAIR QC G3J1X5
CANADA